FLASH and Conventional Radiation Induce Differential Immune Responses in Diffuse Intrinsic Pontine Glioma, Highlighting Potential for Combination Immunotherapy

Oscar Padilla[1#], Hanna E. Minns[2#], Hong-Jian Wei[1], Andrea Webster-Carrion[2], Masih Tazhibi[1], Nicholas M. McQuillan[1], Xu Zhang[3], Rebecca Yeh[2], Zhiguo Zhang[3], Tom K. Hei[1,4], Luca Szalontay[2], Jovana Pavisic[2], Guy Garty[1,4,5], James H. Garvin[2], Peter D. Canoll[6], Claire I. Vanpouille-Box[7], Vilas Menon[8,9,10], Marta Olah[8,9,10], Raul Rabadan[11,12,13], Cheng-Chia Wu[1], Robyn D. Gartrell[2*]

[#]denotes equal contribution

[*]**corresponding author:** Robyn Gartrell, Department of Pediatrics, Columbia University Irving Medical Center, New York, NY, USA. rdg2129@cumc.columbia.edu.

[1]Department of Radiation Oncology, Columbia University Irving Medical Center, New York, NY

[2]Department of Pediatrics, Columbia University Irving Medical Center, New York, NY

[3]Institute for Cancer Genetics, Columbia University Irving Medical Center, New York, NY

[4]Center for Radiological Research, Columbia University Irving Medical Center, New York, NY

[5]Radiological Research Accelerator Facility, Columbia University Irving Medical Center, Irvington, NY.

[6]Department of Pathology and Cell Biology, Columbia University Irving Medical Center, New York, NY

[7]Department of Radiation Oncology, Weill Cornell Medicine, New York, NY

[8]Department of Neurology, Columbia University Irving Medical Center, New York, NY

[9]Center for Translational and Computational Neuroimmunology, Columbia University Irving Medical Center, New York, NY

[10]Taub Institute for Research on Alzheimer's Disease and the Aging Brain, Columbia University Irving Medical Center, New York, NY

[11]Department of Systems Biology, Columbia University Irving Medical Center, New York, NY

[12]Department of Biomedical Informatics, Columbia University Irving Medical Center, New York, NY

[13]Program for Mathematical Genomics, Columbia University Irving Medical Center, New York, NY

Running title: FLASH effect on DIPG immune microenvironment

Keywords: FLASH, DIPG, tumor microenvironment, immune modulation, genome biology, single cell technologies

Funding

This project was funded by the Hyundai Hope on Wheels Hope Scholar Award (PI: R.D.G, Grant #716838) and Swim Across America, including salary support for R.D.G and H.E.M. O.P. received support from the NCI Stimulating Access to Research in Residency (StARR) Award, supplement to the Columbia Cancer Research Program for Resident Investigators (R38CA231577). C-C.W received support from Gary and Yael Fegel Family Foundation (CU21-1080), St. Baldrick's Foundation (SBF CU21-0529), the Star and Storm Foundation, and the Matheson Foundation (UR010590). Development of the FLASH irradiator was partially supported by NIAID Grant U19-AI067773 and by the Departments of Radiation Oncology at Columbia University Irving Medical Center and Weill Cornell Medical Center, as well as by an unrestricted research gift from Barry Neustein. This study used Shared Resources of the Herbert Irving Comprehensive Cancer Center (HICCC) funded in part through Center Grant P30CA013696, specifically Molecular Pathology, Flow Cytometry, Oncology Precision Therapeutics and Imaging (OPTIC), and Genomics and High Throughput Screening Shared Resources. The content is solely the responsibility of the authors and does not necessarily represent the official views of the NIH.

Acknowledgements

We would like to thank Dr. Oren J. Becher for providing the murine DIPG 4423 cell line, and Jim Sharkey, Ron Drake and James Viera for their assistance with the FLASH irradiator including Clinac setup and debugging.

Conflict of Interest Statement

We have no declarations to report.

Data Sharing Statement

Data available upon request to corresponding author Dr. Robyn Gartrell.

ABSTRACT

Purpose

Diffuse Intrinsic Pontine Glioma is a fatal tumor traditionally treated with radiotherapy (RT) and previously characterized as having a non-inflammatory tumor immune microenvironment (TIME). FLASH is a novel RT technique using an ultra-fast dose-rate which is associated with decreased toxicity, effective tumor control and potential immune-sparing properties. However, the effect of FLASH on the DIPG tumor immune microenvironment (TIME) has not yet been explored.

Methods

Here, we perform single-cell RNA sequencing on immune cells isolated from an orthotopic syngeneic murine model of DIPG following the use of FLASH (90Gy/sec) or conventional (2Gy/min) dose-rate RT (CONV-RT), and compare to unirradiated tumor and normal brainstem.

Results

Sequencing of immune cells reveals 17 unique populations, most abundant of which is microglia. In the most activated microglia subtypes, both CONV-RT and FLASH show upregulation of type 1 interferon (IFN1) genes and pathway scores compared to unirradiated tumor. In macrophages (MACs) and dendritic cells (DCs), CONV-RT is significantly enriched for IFN1 while this response is less seen with FLASH. Further, FLASH shows an increase in CNS border-associated MACs and upregulation of a myeloid-derived suppressor cell (MDSC) signature in MONOs, less seen with CONV-RT. In the lymphocytes, FLASH yields a higher mature B cell proportion and upregulation of T-cell activation and trafficking markers compared to CONV-RT. Finally, we correlate our data with myeloid cells from cerebrospinal fluid of human DIPG patients and find overlap with our murine tumor- and treatment-associated markers.

Conclusion

Our work is the first to map CONV-RT and FLASH immune alterations with single-cell resolution in the DIPG TIME. We find that CONV-RT and FLASH sculpt the microglial compartment similarly while recruiting distinct non-resident myeloid subsets and mature B-cell fractions, highlighting the potential to combine each modality with unique immunotherapy regimens in this fatal disease.

INTRODUCTION

Diffuse Intrinsic Pontine Glioma (DIPG), recently re-classified by the World Health Organization (WHO) in 2021 as Diffuse Midline Glioma, H3K27M-altered (DMG), is a universally fatal pediatric brain tumor with a median survival of 9 to 11 months.[1 2] While radiotherapy (RT) is the standard-of-care treatment for DIPG, it is largely palliative, offering temporary relief of symptoms with only a 3 month improvement in survival.[3] Clinical trials have explored a variety of targeted therapies in combination with RT, yet none have prolonged survival.[4]

Immunotherapy is an evolving modality that has radically improved survival in many adult cancers. However, immunotherapies like immune checkpoint inhibitors (ICI) have had minimal success in childhood malignancies.[5] DIPG in particular has been shown to have an immunologically "cold" or non-inflammatory tumor immune microenvironment (TIME), making the use of immunotherapy even more difficult.[6 7] A likely explanation for the non-immunogenic TIME of DIPG is the need to protect the brainstem and its cardiopulmonary regulatory functions from overwhelming inflammation. However, due to this protective tumor location, evaluation of the TIME in DIPG after RT has not been studied leaving a critical gap in determining the potential for combination approaches to improve response to immunotherapy.

While RT has been shown to increase the antigenicity of tumor cells, increase interferon type 1 (IFN1) response and attract tumor-infiltrating lymphocytes,[8 9] it can also deplete immune populations and induce regulatory T-cell phenotypes in the TIME.[10 11] FLASH, or ultra-high dose-rate RT (>40Gy per second), is a novel technique that demonstrates unprecedented normal tissue sparing without compromising tumor control when compared to conventional RT (CONV-RT) dose rates (≤2Gy per minute).[12 13] Prior pre-clinical studies have shown that FLASH, when compared to CONV-RT, yields higher $CD8^+$ T-cells and myeloid subsets in the TIME of Lewis lung carcinoma models[14] while in the brain, decreases microglial activation and neuroinflammation when delivered to tumor-free mice.[15 16] However, no studies to date have investigated the immunomodulatory capacity of FLASH in the DIPG TIME.

In this work, we use single cell RNA sequencing (scRNA-seq) to analyze the TIME in an immunocompetent syngeneic murine model of DIPG post CONV-RT or FLASH and compare to unirradiated tumor and normal brainstem. We also compare our murine myeloid clusters to myeloid cells isolated from the cerebrospinal fluid (CSF) of human DIPG patients treated in a phase I trial using GD2 chimeric antigen receptor (CAR) T-cell therapy.[17] Our work is the first to map CONV-RT and FLASH immune alterations with single-cell resolution in the DIPG TIME and highlights the potential for combining RT and immunotherapy in this cancer.

METHODS

DIPG tumor induction

We utilized a previously published syngeneic murine DIPG cell line (PDGFB+, H3.3K27M, $p53^{-/-}$ cell line, 4423 DIPG, Supplemental Methods).[18] All animal experiments were performed in accordance with national guidelines and approved by our Institutional Animal Care and Use

Committee (IACUC). Five-week-old immunocompetent male B6(Cg)-Tyrc-2J/J mice were purchased from Jackson Laboratories (Bar Harbor, ME). At 6 weeks of age, mice were anesthetized with isoflurane, immobilized in the stereotactic instrument (Stoelting, Wood Dale, IL, USA), and underwent orthotopic implantation with 4423 DIPG at 100,000 cells per microliter (uL) per mouse, prepared in suspension with DMEM (Dulbecco's Modified Eagle's Medium; Corning, 10027CV). Cells were injected at rate of 0.1uL/min using a Hamilton syringe (Hamilton, Darmstadt, Germany) at pontine coordinates of 1mm posterior and 1mm lateral (right) from lambda, and 5.5mm deep. Tumors were confirmed 10 days post injection (dpi), using the Bruker Biospec 9.4 Tesla Small Animal MR Imager (Bruker Medical, Boston, MA, USA) via the Oncology Precision Therapeutics and Imaging Core at our institution.

Radiation

At 17 dpi, tumor-bearing mice were randomly assigned to receive 15Gy of radiation either at conventional dose rate (CONV-RT, 2Gy/min) or at ultra-high dose rate (FLASH, 90Gy/sec) using the Ultra-High Dose-Rate FLASH irradiator at our experimental irradiator facility, based on a repurposed Varian Clinac 2100C.[19] Mice were anesthetized using isoflurane and immobilized using a device incorporating 6.4mm thick adjustable lead shielding, which was aligned to external anatomy creating an open field around the mouse hindbrain. All irradiations were performed using 9MeV electrons (R50=3.9cm). For CONV-RT, mice were individually placed at source to skin distance (SSD) of 171cm and irradiated alongside a National Institute of Standards and Technology (NIST) traceable Advanced Markus Ionization Chamber (AMIC). The CONV-RT dose rate was approximately 2Gy/min and irradiation was stopped when the AMIC reached 15Gy. For FLASH, mice were placed at SSD of 50cm and irradiated with 27-30 pulses of 9MeV electrons at a repetition rate of 180 Hz. Exact positioning of mice and required pulse count for

each irradiation was determined by irradiating the AMIC at the same location prior to mouse irradiation. The built-in ionization chamber was used to verify that there was no drift in beam intensity between calibration and mouse irradiations.

Experimental design and clustering of CD45+ immune cells

Mice were evaluated among four groups: CONV-RT (15Gy at 2Gy/min), FLASH (15Gy at 90Gy/sec), no radiation (Tumor), or normal, healthy mice (Normal Brainstem). Four mice were studied per group for a total of 16 mice. Four days post-RT and 21 dpi, mice were euthanized and brainstems collected for hashtag single cell RNA sequencing (scRNA-seq, Figure 1a, Supplemental Methods) after CD45 isolation to focus on the immune population (Supplemental Methods).

RESULTS

scRNA-seq identifies unique clusters of immune phenotypes in DIPG TIME

Clustering of 33,308 CD45+ cells reveals 17 unique cell subsets (Figure 1b, Supplementary Data 1). We first analyze all clusters in total, agnostic to treatment. We identify four clusters of microglia denoted as MG1, MG2, MG3, and MG4, making up 73.79% of all cells. We find three clusters of non-resident myeloid cells including macrophages (MAC; *Ms4a7*+) at 4.31%, monocytes (MONO; *Lyz2*+) at 2.06% and dendritic cells (DC; *Cd209a*+) at 1.57%. Of the non-myeloid clusters, the most abundant is a mature B cell subtype (BC2; *Igkc*+) at 4.10%. The remaining cells are distributed amongst a T cell cluster (TC; *Cd3d*+) 2.33%, a neutrophil cluster (NEUT; *Ngp*+) 2.00%, a pre-B cell cluster (BC1; *Vpreb3*+) 1.89%, and an natural killer cell cluster (NK; *Klrk1*+) 0.73%. We also report a mixed population of proliferative cells in a cluster defined

by *Mki67* positivity (3.15%) and another mixed population cluster of *S100b*+ cells (1.57%), likely consisting of astrocytes that bypassed CD45 sorting. Lastly, a group of erythrocytes are present based on hemoglobin gene expression (RBC, 0.77%), as well as a cluster of low-quality cells (lq, 1.63%). For individual treatment groups, we examine the proportion of cells coming from each cluster against their total cell number and find variation between groups (Figure 1c, Supplementary Data 1). We perform key marker gene identification for each cell type using differential gene expression analysis, comparing each cluster against all other clusters. From this, we see that each cell type is defined by unique gene signatures and validated by presence of canonical markers (Figure 1d, Supplementary Data 2).

Annotation of microglia reveals four distinct microglial states

Microglia are defined by expression of canonical genes such as *P2ry12, Siglech* and *Tmem119*,[20] [21] and resolve into four distinct subtypes (M1, M2, M3, and MG4) based on unique marker gene sets (Supplemental Figure 1a). Expression of *P2ry12*, associated with homeostasis, decreases from MG1 to MG4; while expression of *Apoe*, a marker of microglial activation, increases in microglia within or proximal to MG3 and MG4 (Supplemental Figure 1b).[21] [22] MG1 and MG2 share similar profiles, with MG2 showing higher expression of *Apoe* and *Cdkn1a* (Supplementary Data 2). MG3 is enriched for multiple interferon genes such as *Isg15* and *Ifit3* (Supplemental Figure 1c). When we run the top 50 differentially expressed genes in MG3 through REACTOME for pathway analysis (Supplemental Methods), the top 3 pathways consist of interferon alpha/beta signaling, interferon signaling, and immune cytokine signaling (Supplemental Figure 1c). MG4 shows high expression of metabolism-associated genes such as *Lpl* (lipoprotein lipase) and *Fabp5* (fatty-acid binding protein) (Supplemental Figure 1d). When running the top 50 genes from MG4 through

REACTOME, the 10 most significant pathways include neutrophil degranulation, interleukin-10 signaling, glucose metabolism, and iron uptake (Supplemental Figure 1d).

Treatment groups differentially induce microglia clusters

In Normal Brainstem, MG1 and MG2 account for the majority of microglia (44.5% and 47.0% respectively), with less than 10% of cells present in MG3 and MG4 clusters (Figure 2a, b). In the presence of tumor, without irradiation (Tumor), there is an expansion of MG4 (30.8%) while MG3 (4.85%) is maintained at a similar proportion as in Normal Brainstem (Figure 2b). Upon irradiation with either CONV-RT or FLASH, the MG3 cluster undergoes significant expansion (17.0% and 16.2% respectively), while MG4 experiences moderate reduction (26.7% and 22.3% respectively) compared to Tumor (Figure 2b).

We next perform two individual analyses to identify genomic alterations uniquely induced by FLASH and by CONV-RT relative to Tumor (FvT and CvT, respectively; Supplementary Data 3). We compare both the common and the different up- and down-regulated genes resulting from each analysis. For all MG clusters, both RT modalities upregulate DNA damage response genes associated with ionizing radiation (i.e. *Cdkn1a*, *Phlda3*, *Bax*) to a similar extent (Figure 2c-d, Supplemental Figure 2a-b).[23,24] In MG1 and MG2, FLASH and CONV-RT similarly downregulate innate immunity chemokines *Ccl9* and *Ccl6* compared to Tumor (Supplemental Figure 2a). In MG3, both RT interventions similarly downregulate *Ccl9* along with *Klf2* (Figure 2c), a myeloid repressor of neuroinflammation.[25] In MG4, both RT groups similarly upregulate type 1 interferon (IFN1) genes such as *Isg15, Ifitm3*, and *Ifit3*, while decreasing expression of major histocompatibility complex (MHC) class II genes *H2-Aa* and *H2-Ab1* compared to Tumor (Figure 2c-d). We run the most significant, upregulated common genes between FvT and CvT for each MG cluster through REACTOME and find pathways associated with cell cycle checkpoints and

DNA damage response (Figure 2d, Supplemental Figure 2b). For MG4 specifically, we also find common pathways relating to interferon alpha/beta signaling and cytokine signaling (Figure 2d). Regarding differential upregulation of genes, FLASH shows unique enrichment for *Apoe* (MG1, MG3) and *Ccl12* (MG1, MG2), while CONV-RT shows distinct increases in *Cd52*, *Ifi27l2a*, *Ccl2*, and *Cst7* in MG4 (Supplementary Data 3).

Characterization of non-resident myeloid clusters and FLASH effect in the monocyte population

We next examine the non-resident myeloid clusters: MONO, MAC, and DC, and find clear segmentation of gene signatures, with varying degrees of overlap in classical myeloid markers such as *Ccr2* and *Vim*[26 27], and MHC class II genes *H2-Ab1* and *Cd74* (Figure 3a). We observe that MONOs share similar canonical markers with DCs, which are upregulated for antigen presentation (*H2-Ab1*, *H2-Eb1*, *H2-Aa*, *Cd74*); while MACs have a more variable signature. Studying the density and proportion of MACs, DCs and MONOs within the non-resident myeloid compartment of each treatment group, we find treatment-specific differences (Figure 3b-c). Specifically, we find that in CONV-RT, MACs represent the highest proportion of cells (70.3%) within the non-resident myeloid population specific to this treatment group. Extending this analysis to the other groups, we find that FLASH has 53.6%, Tumor has 52.1% and Normal Brainstem has 36.5% MACs within their respective non-resident myeloid totals. For DC proportions, FLASH has 26.5%, CONV-RT has 16.7%, Tumor has 18.4% and Normal Brainstem has 21.6%. For MONOs, FLASH has 19.8%, CONV-RT has 13.1%, Tumor has 29.5% and Normal Brainstem has 41.8% (Figure 3b-c).

We then perform differential gene expression analysis within the non-resident myeloid clusters between individual RT groups and Tumor (FvT and CvT; Supplementary Data 3). In the MONO

population, we find that there is almost no differential gene expression between CONV-RT and Tumor, barring *Spp1*, which is enriched in the former group (Supplementary Data 3). However, FLASH has a strikingly different MONO profile than Tumor - including increased expression of *Clec4a1* and *Clec4a3*, and decreased expression of complement family genes *C1qa*, *C1qb*, and *C1qc* (Figure 3d). To further define the MONO cluster, we calculate a monocyte-derived suppressor cell (MDSC) signature score using ssGSEA applied to MONOs from the different treatment groups, and find that FLASH is significantly enriched for this signature compared to CONV-RT and Tumor (both $p<0.0001$) (Figure 3e).

CONV-RT and FLASH show differential interferon activation in macrophages and dendritic cells

Next, we conduct FvT and CvT analyses in the MAC cluster and find similarly upregulated genes associated with RT response (e.g. *Cdkn1a*, *Bax*, and *Phlda3*)[23] [24] as well as similarly downregulated genes associated with antigen presentation (e.g. *Cd74, H2-Eb1, H2-Aa, H2-Ab1*) (Figure 4a). We then analyze the genes that are specifically upregulated in either FvT or CvT but not the other. For CONV-RT, the most upregulated genes versus Tumor include *Isg15, Irf7, Ifit3, Ifit2, Tgfbi*, and *Tspo* (Figure 4b). For FLASH, the most upregulated genes are *Mrc1*, *Pf4*, *Lyve1* and *Cd163*. Mapping the average expression of these genes onto non-resident myeloid clusters, we find a dichotomy between CONV-RT- (left 4 plots) and FLASH-associated (right 4 plots) MACs (Figure 4c). Evaluating interferon response, we find that CONV-RT MACs have a significantly higher interferon alpha/beta signaling (IFN1) score than FLASH and Tumor (both $p < 0.0001$) (Figure 4d). Analyzing FvT cells in the DC cluster, we find only a few genes that are differentially expressed in FLASH compared to Tumor (upregulated: *Clec4b1, Pid1;* downregulated: *Mdh2, Il1b, Cdk2ap2)* (Supplementary Data 3). Conversely, CvT has many

differentially expressed genes (Figure 4e), with a robust increase in interferon related genes such as *Isg15, Irf7, Ifit3,* and *Ifit2,* and significant enrichment of IFN1 compared to FLASH and Tumor (both $p < 0.0001$) (Figure 4f).

Characterization of lymphocyte clusters

NK, T- and B-cells are defined by canonical genes (Supplemental Figure 3a) and account for 9.05% of the total immune population. The proportion of T-cells varied between groups, with Tumor having 3.08% of total immune cells, CONV-RT 1.89% and FLASH 2.00% (Supplementary Data 1). On FvT and CvT analyses, we find that FLASH upregulates *Lck, Klf2, Sell, and Lef1* in T-cells relative to Tumor (Supplemental Figure 3b). These genes are not increased for CONV-RT compared to tumor. Analysis of B-cells demonstrates highest proportion of BC2 cells - enriched for maturation marker *Ms4a1* and immunoglobulin genes (e.g., *Ighd, Iglc2*)[28] - in FLASH (5.57%) versus <2% in both CONV-RT (1.95%) and Tumor (1.46%) (Supplementary Data 1). There were few genes differentially enriched for FvT and none for CvT among BC2 cells (Supplementary Data 3). NK cell and BC1 proportions were less than 1% across tumor groups and thus not suitable for differential expression analysis (Supplementary Data 1).

Evaluation of myeloid cells from cerebrospinal fluid (CSF) of DIPG patients treated with GD2-CAR T cell therapy

After pre-processing and batch correction of 2,257 CSF myeloid cells, clustering reveals 7 unique populations including MONOs, DCs, and 5 other myeloid subsets defined by key marker genes (Figure 5a, Supplementary Data 4). We use the top 50 genes characterizing each of our murine myeloid clusters (MG1-4 and non-resident myeloid cells) to generate enrichment scores for each of these within cells from the human myeloid dataset (Figure 5b-c, Supplemental Figure 4).

Next, we evaluate differential gene expression between murine Tumor and Normal Brainstem groups in order to generate murine Tumor-associated MG and non-resident myeloid signatures. We cross-reference these signatures with the top 50 markers from human DIPG myeloid clusters and visualize gene overlaps (Figure 5d), which include *Apoe, Ccl4, Cd52, Ccl3, Fth1* and *Ifitm3* for murine Tumor-associated MG; and *Ctsd, Cd9, Lgmn, Mafb, Il1b,* and *Trem2* for murine Tumor-associated non-resident myeloid cells; with *Spp1* similarly overlapped in both (Figure 5d, Supplementary Data 5). The same cross-referencing is done using top upregulated markers in murine non-resident myeloid cells as identified in the previous CvT and FvT analyses (Figure 5e). The overlap includes *Isg15, Ifit3, Ifit2,* and *Ifit1* for murine CONV-RT-associated non-resident myeloid cells; and *Mrc1, F13a1,* and *Clec10a* for murine FLASH-associated non-resident myeloid cells; with *Pla2g7* similarly overlapped in both (Supplementary Data 6). Conducting this analysis in murine MG cells, there are only a few genes that overlap, including *Ifit3* and *Isg15* for murine CONV-RT-associated MG, and *Ccl2* for murine FLASH-associated MG; with *Ifitm3* similarly overlapped in both (Supplementary Data 6).

DISCUSSION

This work is the first to evaluate the RT immune response in DIPG and compare RT dose rates in the TIME of an immunocompetent syngeneic murine model of DIPG. Previous work demonstrates a non-inflammatory TIME in human DIPG at diagnosis.[6] However, these prior analyses are composed primarily of biopsy specimens - as human DIPGs are not resectable - and therefore unlikely to be representative of the overall TIME. Considering that biopsies are not typically obtained after RT in humans, our study offers a unique perspective into the RT immune response in the DIPG TIME.

Consistent with previous work, our scRNA-seq analysis finds that the immune landscape of DIPG is largely composed of microglial populations and a small subset of non-resident myeloid cells and lymphocytes.[6] In tumor groups, with or without RT, we see a phenotypic continuum from homeostatic MG1 and MG2 to more activated microglial states in MG4, as depicted by the increasing expression gradients of *Apoe, Spp1, Lpl,* and *Fabp5,* and enrichment of interleukin-10 signaling, glucose metabolism and iron uptake pathways along this MG trajectory. The literature ascribes this spectrum of genes and metabolic pathways culminating in MG4 to disease- and injury-associated microglial states.[22 29] Moreover, we see that following irradiation with either FLASH or CONV-RT, an interferon-associated microglia subtype emerges – MG3 – showing characteristic expression of IFN1 genes and pathways.[30] Interestingly, MG4 also manifests interferon gene and pathway expression, and suggests that disease-associated microglia retain some capacity for immune activation in the setting of RT. While previous work shows that FLASH activates microglia less than CONV-RT in tumor-free mice, our work demonstrates that these two dose rates activate microglia to a similar extent in DIPG.[15 31]

Despite similarities in the predominant microglial population, we find marked differences between FLASH and CONV-RT in the MAC cluster, which dichotomizes into distinct subtypes based on RT modality. In the setting of CONV-RT, the most upregulated genes, *Isg15, Ifit3, Cxcl10,* indicate robust interferon and pro-inflammatory responses.[32] *Tgfbi* is also upregulated in CONV-RT and is consistent with prior reports in this dose-rate context showing high levels of TGF-β induction, which has been previously linked to immunosuppression and progression of high-grade gliomas.[33 34] In the setting of FLASH, MACs show an increase in *Cd163,* which is also associated with an immunosuppressive phenotype, as well as classical markers of CNS border-associated macrophages - *Mrc1* (Cd206), *Pf4,* and *Lyve1*.[21 32 35] This finding indicates that MACs likely arise

from proximal monocyte progenitor niches in CNS border tissues post-FLASH, which spares in-field organs-at-risk better, while CONV-RT mostly recruits MACs via extracranial bone-marrow progentiors.[36] Notably, though CONV-RT MACs express high levels of interferon and the monocytic progenitors in this group also express Spp1, which is associated with pro-tumoral phenotypes in high-grade gliomas.[37]

Similar to MACs, we find that CONV-RT elicits a robust interferon program in DCs, which are critical mediators of anti-tumoral T-cell responses following radiation.[8 9] FLASH, on the other hand, evokes a unique DC phenotype described by receptor Clec4b1, which has been previously linked to activation of IFN-γ effector T-cells.[38] While the origin of these DC subsets remains to be specified, MONOs in FLASH, when compared to CONV-RT, show a bias away from DC differentiation and towards a MAC fate as reflected by the upregulation of *Clec4a1* and *Clec4a3*.[39] [40] This lineage bias may reflect early-state inflammation in which immature MONOs preferentially differentiate into MACs, particularly of the M2 phenotype when infiltrating the brain, and hints at a possible temporal and/or qualitative difference in the inflammatory cascade between CONV-RT and FLASH.[41 42] The MDSC signature enrichment observed in FLASH may also be understood in the context of early-state inflammation, in which "emergency" myelopoiesis following an inflammatory cue leads to mobilization of immature MONOs to the TIME where they exert immune regulation ("suppression") upon sustained accumulation.[43] In this scenario, FLASH may differentially spare vascular integrity and myeloid precursors in the cranial bone marrow, leading to higher migration and steady-state accumulation of MONOs in the TIME. Recent work in a lung cancer model similarly demonstrates low and high monocytic infiltration in the TIME following CONV-RT and FLASH, respectively.[44]

Though previous FLASH studies have shown an increase in T-cells, we only see a marginally higher proportion of T-cells in FLASH versus CONV-RT.[14 44] This may be due to the lympho-depleted state of the DIPG TIME at baseline.[6] It is also possible that our interrogation time point of 4 days post-RT may be too early to capture peak T-cell TIME infiltration, as previous studies have evaluated T-cell presence at day 14 after irradiation.[45] Though the scarcity of T-cell populations does not allow for statistically tractable comparisons between CD4 and CD8 T-cells, we find that FLASH significantly upregulates genes involved in T-cell activation (*Lck*) and trafficking (*Klf2*), which occurs on the background of higher central-memory (*Sell, Lef1, Klf2*) and naïve (*Sell, Lef1, Ccr7*) T-cell states suggesting a possible differential recruitment of these cells from the periphery.[46 47] When evaluating B cell clusters, we observe a higher mature B cell (BC2) fraction in FLASH compared to CONV-RT and Tumor groups, suggesting that ultra-high dose-rate irradiation may potently elicit B-cell differentiation peri/intratumorally. Mature B cells have been recently observed in tertiary lymphoid structures surrounding brain metastases, where they differentiate into plasma cells, and have been previously linked to improved ICI responses in human patients.[28 48]

To understand the clinical relevance of our findings, we evaluate myeloid cells isolated from CSF of human DIPG patients who received treatment with GD2-CAR T-cell therapy.[17] In this analysis, we see 15 genes that overlap in CSF and murine DIPG tumor, including *Trem2*, which is a pro-tumoral marker in tumor-associated MACs linked to inferior ICI responses.[49] We also find overlapping interferon markers (*Isg15, Ifit3, Ifit2, Ifit1*) between non-resident myeloid cells from CONV-irradiated mice and human CSF post GD2-CAR T-cell therapy. These treatment-related markers do not overlap with non-resident myeloid cells from FLASH-irradiated mice, possibly because the human CSF cells were procured from patients who previously received CONV-RT.

In summary, we find that both resident and non-resident immune cells in the DIPG TIME can mount an IFN1 response post RT, which is a critical feature of tumors that typically respond to immunotherapy.[9] This IFN1 response is equally seen between CONV-RT and FLASH in microglia, and more frequently following CONV-RT in non-resident myeloid cells, specifically DCs and MACs. The latter observation highlights the opportunity to combine CONV-RT with immunotherapies that leverage the non-resident myeloid compartment. Although less of an IFN1 response is seen in the non-resident myeloid compartment with FLASH, excessive immune recruitment, especially in the brainstem, can be a double-edged sword as neuroinflammation can be fatal and is associated with neurocognitive dysfunction in children.[50] As such, the use of FLASH may be beneficial in younger patients who wouldn't typically receive RT or patients with an elevated state of inflammation, such as patients receiving GD2-CAR T-cell therapy, who are at risk for developing tumor inflammation-associated neurotoxicity requiring intensive care monitoring.[17] Moreover, considering the relative lympho-stimulating effect of FLASH, this modality may also be better suited for immunotherapies targeting lymphocytes. An important limitation of this work is that the analysis is restricted to a single time point of 4 days after a single 15Gy dose. Further studies that evaluate the impact of RT dose rate on the DIPG TIME and on control and survival endpoints using clinically relevant doses and schedules are needed to understand how and when to incorporate immunotherapies in future human clinical trials.

REFERENCES

1. Cooney T, Lane A, Bartels U, et al. Contemporary survival endpoints: an International Diffuse Intrinsic Pontine Glioma Registry study. *Neuro Oncol* 2017;19(9):1279-80. doi: 10.1093/neuonc/nox107 [published Online First: 2017/08/20]
2. Louis DN, Perry A, Wesseling P, et al. The 2021 WHO Classification of Tumors of the Central Nervous System: a summary. *Neuro Oncol* 2021;23(8):1231-51. doi: 10.1093/neuonc/noab106
3. Johung TB, Monje M. Diffuse Intrinsic Pontine Glioma: New Pathophysiological Insights and Emerging Therapeutic Targets. *Curr Neuropharmacol* 2017;15(1):88-97. doi: 10.2174/1570159x14666160509123229

4. Long W, Yi Y, Chen S, et al. Potential New Therapies for Pediatric Diffuse Intrinsic Pontine Glioma. *Front Pharmacol* 2017;8:495. doi: 10.3389/fphar.2017.00495 [published Online First: 2017/08/10]
5. Long AH, Morgenstern DA, Leruste A, et al. Checkpoint Immunotherapy in Pediatrics: Here, Gone, and Back Again. *Am Soc Clin Oncol Educ Book* 2022;42:1-14. doi: 10.1200/EDBK_349799
6. Lin GL, Nagaraja S, Filbin MG, et al. Non-inflammatory tumor microenvironment of diffuse intrinsic pontine glioma. *Acta Neuropathol Commun* 2018;6(1):51. doi: 10.1186/s40478-018-0553-x [published Online First: 2018/06/30]
7. Price G, Bouras A, Hambardzumyan D, et al. Current knowledge on the immune microenvironment and emerging immunotherapies in diffuse midline glioma. *EBioMedicine* 2021;69:103453. doi: 10.1016/j.ebiom.2021.103453 [published Online First: 2021/06/23]
8. De Martino M, Padilla O, Daviaud C, et al. Exploiting Radiation Therapy to Restore Immune Reactivity of Glioblastoma. *Front Oncol* 2021;11:671044. doi: 10.3389/fonc.2021.671044 [published Online First: 2021/06/08]
9. Vanpouille-Box C, Alard A, Aryankalayil MJ, et al. DNA exonuclease Trex1 regulates radiotherapy-induced tumour immunogenicity. *Nat Commun* 2017;8:15618. doi: 10.1038/ncomms15618 [published Online First: 2017/06/10]
10. Yovino S, Kleinberg L, Grossman SA, et al. The etiology of treatment-related lymphopenia in patients with malignant gliomas: modeling radiation dose to circulating lymphocytes explains clinical observations and suggests methods of modifying the impact of radiation on immune cells. *Cancer Invest* 2013;31(2):140-4. doi: 10.3109/07357907.2012.762780 [published Online First: 2013/02/01]
11. Heylmann D, Ponath V, Kindler T, et al. Comparison of DNA repair and radiosensitivity of different blood cell populations. *Sci Rep* 2021;11(1):2478. doi: 10.1038/s41598-021-81058-1 [published Online First: 2021/01/30]
12. Montay-Gruel P, Petersson K, Jaccard M, et al. Irradiation in a flash: Unique sparing of memory in mice after whole brain irradiation with dose rates above 100Gy/s. *Radiother Oncol* 2017;124(3):365-69. doi: 10.1016/j.radonc.2017.05.003 [published Online First: 2017/05/27]
13. Montay-Gruel P, Bouchet A, Jaccard M, et al. X-rays can trigger the FLASH effect: Ultra-high dose-rate synchrotron light source prevents normal brain injury after whole brain irradiation in mice. *Radiother Oncol* 2018;129(3):582-88. doi: 10.1016/j.radonc.2018.08.016 [published Online First: 2018/09/05]
14. Rama N ST, Shukla S, Goda C, Milewski D, Mascia AE, Vatner RE, Sengupta D, Katsis A, Abel E, Girdhani S, Miyazaki M, Rodriguez A, Ku A, Dua R, Parry R, Kalin TV. Improved Tumor Control Through T-cell Infiltration Modulated by Ultra-High Dose Rate Proton FLASH Using a Clinical Pencil Beam Scanning Proton System. *International Journal of Radiation Oncology, Biology, Physics* 2019;105(1):S164-S65. doi: https://doi.org/10.1016/j.ijrobp.2019.06.187
15. Alaghband Y, Cheeks SN, Allen BD, et al. Neuroprotection of Radiosensitive Juvenile Mice by Ultra-High Dose Rate FLASH Irradiation. *Cancers (Basel)* 2020;12(6) doi: 10.3390/cancers12061671 [published Online First: 2020/07/01]
16. Zhang Y, Ding Z, Perentesis JP, et al. Can Rational Combination of Ultra-high Dose Rate FLASH Radiotherapy with Immunotherapy Provide a Novel Approach to Cancer Treatment? *Clin Oncol (R Coll Radiol)* 2021;33(11):713-22. doi: 10.1016/j.clon.2021.09.003 [published Online First: 2021/09/24]
17. Majzner RG, Ramakrishna S, Yeom KW, et al. GD2-CAR T cell therapy for H3K27M-mutated diffuse midline gliomas. *Nature* 2022;603(7903):934-41. doi: 10.1038/s41586-022-04489-4 [published Online First: 2022/02/08]
18. Cordero FJ, Huang Z, Grenier C, et al. Histone H3.3K27M Represses p16 to Accelerate Gliomagenesis in a Murine Model of DIPG. *Mol Cancer Res* 2017;15(9):1243-54. doi: 10.1158/1541-7786.MCR-16-0389 [published Online First: 2017/05/20]

19. Garty G DN, Obaid R, Brenner D, Kachnic L. EPD038 - THE FLASH IRRADIATOR AT THE RADIOLOGICAL RESEARCH ACCELERATOR FACILITY. Physica Medica, 2022.
20. Hickman SE, Kingery ND, Ohsumi TK, et al. The microglial sensome revealed by direct RNA sequencing. *Nat Neurosci* 2013;16(12):1896-905. doi: 10.1038/nn.3554 [published Online First: 2013/10/29]
21. Ochocka N, Segit P, Walentynowicz KA, et al. Single-cell RNA sequencing reveals functional heterogeneity of glioma-associated brain macrophages. *Nat Commun* 2021;12(1):1151. doi: 10.1038/s41467-021-21407-w [published Online First: 2021/02/21]
22. Keren-Shaul H, Spinrad A, Weiner A, et al. A Unique Microglia Type Associated with Restricting Development of Alzheimer's Disease. *Cell* 2017;169(7):1276-90 e17. doi: 10.1016/j.cell.2017.05.018 [published Online First: 2017/06/13]
23. Kumar A, Ghosh S, Chandna S. Evidence for microRNA-31 dependent Bim-Bax interaction preceding mitochondrial Bax translocation during radiation-induced apoptosis. *Sci Rep* 2015;5:15923. doi: 10.1038/srep15923 [published Online First: 2015/10/31]
24. Osman AM, Sun Y, Burns TC, et al. Radiation Triggers a Dynamic Sequence of Transient Microglial Alterations in Juvenile Brain. *Cell Rep* 2020;31(9):107699. doi: 10.1016/j.celrep.2020.107699 [published Online First: 2020/06/04]
25. Shi H, Sheng B, Zhang C, et al. Myeloid Kruppel-like factor 2 deficiency exacerbates neurological dysfunction and neuroinflammation in a murine model of multiple sclerosis. *J Neuroimmunol* 2014;274(1-2):234-9. doi: 10.1016/j.jneuroim.2014.06.023 [published Online First: 2014/07/24]
26. Merah-Mourah F, Cohen SO, Charron D, et al. Identification of Novel Human Monocyte Subsets and Evidence for Phenotypic Groups Defined by Interindividual Variations of Expression of Adhesion Molecules. *Sci Rep* 2020;10(1):4397. doi: 10.1038/s41598-020-61022-1 [published Online First: 2020/03/12]
27. Crane MJ, Daley JM, van Houtte O, et al. The monocyte to macrophage transition in the murine sterile wound. *PLoS One* 2014;9(1):e86660. doi: 10.1371/journal.pone.0086660 [published Online First: 2014/01/28]
28. Patil NS, Nabet BY, Muller S, et al. Intratumoral plasma cells predict outcomes to PD-L1 blockade in non-small cell lung cancer. *Cancer Cell* 2022;40(3):289-300 e4. doi: 10.1016/j.ccell.2022.02.002 [published Online First: 2022/02/27]
29. Hammond TR, Dufort C, Dissing-Olesen L, et al. Single-Cell RNA Sequencing of Microglia throughout the Mouse Lifespan and in the Injured Brain Reveals Complex Cell-State Changes. *Immunity* 2019;50(1):253-71 e6. doi: 10.1016/j.immuni.2018.11.004 [published Online First: 2018/11/26]
30. Lee PY, Li Y, Kumagai Y, et al. Type I interferon modulates monocyte recruitment and maturation in chronic inflammation. *Am J Pathol* 2009;175(5):2023-33. doi: 10.2353/ajpath.2009.090328 [published Online First: 2009/10/08]
31. Simmons DA, Lartey FM, Schuler E, et al. Reduced cognitive deficits after FLASH irradiation of whole mouse brain are associated with less hippocampal dendritic spine loss and neuroinflammation. *Radiother Oncol* 2019;139:4-10. doi: 10.1016/j.radonc.2019.06.006 [published Online First: 20190625]
32. Gjorgjevski M, Hannen R, Carl B, et al. Molecular profiling of the tumor microenvironment in glioblastoma patients: correlation of microglia/macrophage polarization state with metalloprotease expression profiles and survival. *Biosci Rep* 2019;39(6) doi: 10.1042/BSR20182361 [published Online First: 2019/05/31]
33. Favaudon V, Caplier L, Monceau V, et al. Ultrahigh dose-rate FLASH irradiation increases the differential response between normal and tumor tissue in mice. *Sci Transl Med* 2014;6(245):245ra93. doi: 10.1126/scitranslmed.3008973 [published Online First: 2014/07/18]
34. Han J, Alvarez-Breckenridge CA, Wang QE, et al. TGF-beta signaling and its targeting for glioma treatment. *Am J Cancer Res* 2015;5(3):945-55. [published Online First: 2015/06/06]

35. Jordao MJC, Sankowski R, Brendecke SM, et al. Single-cell profiling identifies myeloid cell subsets with distinct fates during neuroinflammation. *Science* 2019;363(6425) doi: 10.1126/science.aat7554 [published Online First: 2019/01/27]
36. Utz SG, Greter M. Checking macrophages at the border. *Nat Neurosci* 2019;22(6):848-50. doi: 10.1038/s41593-019-0411-6 [published Online First: 2019/05/08]
37. Wei J, Marisetty A, Schrand B, et al. Osteopontin mediates glioblastoma-associated macrophage infiltration and is a potential therapeutic target. *J Clin Invest* 2019;129(1):137-49. doi: 10.1172/JCI121266 [published Online First: 2018/10/12]
38. Toyonaga K, Torigoe S, Motomura Y, et al. C-Type Lectin Receptor DCAR Recognizes Mycobacterial Phosphatidyl-Inositol Mannosides to Promote a Th1 Response during Infection. *Immunity* 2016;45(6):1245-57. doi: 10.1016/j.immuni.2016.10.012 [published Online First: 2016/11/27]
39. Fujikado N, Saijo S, Yonezawa T, et al. Dcir deficiency causes development of autoimmune diseases in mice due to excess expansion of dendritic cells. *Nat Med* 2008;14(2):176-80. doi: 10.1038/nm1697 [published Online First: 2008/01/22]
40. Park I, Goddard ME, Cole JE, et al. C-type lectin receptor CLEC4A2 promotes tissue adaptation of macrophages and protects against atherosclerosis. *Nat Commun* 2022;13(1):215. doi: 10.1038/s41467-021-27862-9 [published Online First: 2022/01/13]
41. Auffray C, Fogg D, Garfa M, et al. Monitoring of blood vessels and tissues by a population of monocytes with patrolling behavior. *Science* 2007;317(5838):666-70. doi: 10.1126/science.1142883 [published Online First: 2007/08/04]
42. Saederup N, Cardona AE, Croft K, et al. Selective chemokine receptor usage by central nervous system myeloid cells in CCR2-red fluorescent protein knock-in mice. *PLoS One* 2010;5(10):e13693. doi: 10.1371/journal.pone.0013693 [published Online First: 2010/11/10]
43. Gabrilovich DI, Nagaraj S. Myeloid-derived suppressor cells as regulators of the immune system. *Nat Rev Immunol* 2009;9(3):162-74. doi: 10.1038/nri2506 [published Online First: 2009/02/07]
44. Kim YE, Gwak SH, Hong BJ, et al. Effects of Ultra-high doserate FLASH Irradiation on the Tumor Microenvironment in Lewis Lung Carcinoma: Role of Myosin Light Chain. *Int J Radiat Oncol Biol Phys* 2021;109(5):1440-53. doi: 10.1016/j.ijrobp.2020.11.012 [published Online First: 2020/11/14]
45. Filatenkov A, Baker J, Mueller AM, et al. Ablative Tumor Radiation Can Change the Tumor Immune Cell Microenvironment to Induce Durable Complete Remissions. *Clin Cancer Res* 2015;21(16):3727-39. doi: 10.1158/1078-0432.CCR-14-2824 [published Online First: 2015/04/15]
46. Lovatt M, Filby A, Parravicini V, et al. Lck regulates the threshold of activation in primary T cells, while both Lck and Fyn contribute to the magnitude of the extracellular signal-related kinase response. *Mol Cell Biol* 2006;26(22):8655-65. doi: 10.1128/MCB.00168-06 [published Online First: 2006/09/13]
47. Szabo PA, Levitin HM, Miron M, et al. Single-cell transcriptomics of human T cells reveals tissue and activation signatures in health and disease. *Nat Commun* 2019;10(1):4706. doi: 10.1038/s41467-019-12464-3 [published Online First: 2019/10/19]
48. Biermann J, Melms JC, Amin AD, et al. Dissecting the treatment-naive ecosystem of human melanoma brain metastasis. *Cell* 2022;185(14):2591-608 e30. doi: 10.1016/j.cell.2022.06.007 [published Online First: 2022/07/09]
49. Molgora M, Esaulova E, Vermi W, et al. TREM2 Modulation Remodels the Tumor Myeloid Landscape Enhancing Anti-PD-1 Immunotherapy. *Cell* 2020;182(4):886-900 e17. doi: 10.1016/j.cell.2020.07.013 [published Online First: 20200811]
50. Walter AW, Mulhern RK, Gajjar A, et al. Survival and neurodevelopmental outcome of young children with medulloblastoma at St Jude Children's Research Hospital. *J Clin Oncol* 1999;17(12):3720-8. doi: 10.1200/JCO.1999.17.12.3720 [published Online First: 1999/11/30]

MAIN FIGURE LEGENDS

Figure 1: Experimental design and clustering of CD45+ cells. (a) Day 0; H3.3K27M mutant cells are stereotactically injected into the brainstem of juvenile mice. Day 10; tumor presence is confirmed by MRI. Day 17; mice are randomly assigned to receive either conventional radiation (RT) (CONV-RT, 15Gy at 2Gy/min), FLASH (15Gy at 90Gy/sec), or no RT (Tumor). Day 21; all groups – including a Normal Brainstem cohort - are euthanized for cell isolation, hashtag oligonucleotide (HTO) staining, CD45+ sorting, and finally, single-cell RNA sequencing. **(b)** Clustering of 33,308 CD45+ cells reveals 17 unique cell subsets. **(c)** Cluster proportions making up each treatment group when evaluated against the total number of cells collected for that specific group. **(d)** Key marker genes for each cluster.

Figure 2: Localization of treatment groups across microglia clusters. (a) Density of cells from each treatment group visualized across microglia (MG) clusters. **(b)** MG cluster proportions within each treatment group, determined as the fraction of MG subtype cells over the total number of microglia cells collected for that specific group. **(c)** Common up- and down-regulated genes between independent differential expression analyses of CONV-RT vs Tumor (white) and FLASH vs Tumor (green) in MG3 and MG4, plotted by average log2 fold change. **(d)** REACTOME pathway analysis of common upregulated genes between independent differential expression analyses of CONV-RT vs Tumor and FLASH vs Tumor in MG3 (pink) and MG4 (turquoise). Significance of the pathway analysis is reported using–log2 of the false discovery rate (FDR) and the percentage of entities found in the gene list inputted compared to the total number of genes in each pathway.

Figure 3: Characterization of non-resident myeloid clusters and evaluation of treatment groups within monocyte population. (a) Heatmap of top marker genes representing monocytes (MONO), macrophages (MAC), and dendritic cells (DC). **(b)** Density of cells coming from each treatment group visualized across non-resident myeloid clusters. **(c)** Non-resident myeloid subtype proportions within each treatment group, determined as the fraction of subtype cells over the total number of non-resident myeloid cells collected for that specific group. **(d)** Volcano plot denoting differential gene expression between FLASH vs Tumor in the MONO cluster. Gray vertical lines indicate average log2 fold change of 0.8 and horizontal gray line indicates adjusted p-value <0.05. **(e)** Single sample gene set enrichment (ssGSEA) analysis of the cells from CONV-RT, FLASH and Tumor groups in the MONO cluster using a monocyte-derived suppressor-cell (MDSC) gene set (**** = $p<0.0001$, ns = not significant).

Figure 4: Subanalysis of macrophage and dendritic cell populations. (a) Common up- and down-regulated genes between independent differential expression analyses of CONV-RT vs Tumor (white) and FLASH vs Tumor (green) in the MAC cluster, plotted by average log2 fold change. **(b)** Volcano plot of the upregulated genes in CONV-RT vs Tumor (left) and FLASH vs Tumor (right) in the MAC cluster. Gray vertical lines indicate average log2 fold change of 0.8 and horizontal gray line indicates adjusted p-value <0.05. **(c)** Feature plots of the average expression of top upregulated genes in CONV-RT vs Tumor (left) and FLASH vs Tumor (right) across non-resident myeloid clusters. **(d)** ssGSEA analysis of MACs from CONV-RT, FLASH and Tumor groups using REACTOME interferon alpha/beta (IFN1) gene set (**** = $p<0.0001$, ** = $p< 0.01$). **(e)** Dot plot of top 20 most upregulated genes in CONV-RT vs Tumor and the two

significantly upregulated genes in FLASH vs Tumor (Pid1, Clec4b1) in DCs. **(f)** ssGSEA analysis of DCs from CONV-RT, FLASH and Tumor groups using IFN1 gene set (**** = $p<0.0001$, ns = not significant).

Figure 5: Evaluation of myeloid cells from CSF of human DIPG patients treated with GD2-CAR T cell therapy. (a) Clustering of 2,257 myeloid cells reveals 7 unique clusters. **(b)** (Top) Feature plot of enrichment scores generated in the human myeloid cells using the top 50 genes from the murine MG4 cluster. (Bottom) Violin plot representing these same enrichment scores for murine MG4 within each human myeloid cluster. **(c)** (Top) Feature plot of enrichment scores generated in human myeloid cells using the top 50 genes from the murine MONO cluster. (Bottom) Violin plot representing these same enrichment scores for murine MONO in each human myeloid cluster. **(d)** (Top) Venn diagram of overlapping genes from murine Tumor-associated MG signature (left, yellow), murine Tumor-associated non-resident myeloid signature (right, violet), and the top 50 genes from human myeloid clusters (center, light pink). (Bottom) Dot plot of the expression of these overlapping genes in Tumor and Normal Brainstem in murine MG (left, yellow) and murine non-resident myeloid cells (right, violet). **(e)** (Top) Venn diagram of overlapping genes from murine CONV-RT-associated non-resident myeloid signature (left, blue), murine FLASH-associated non-resident myeloid signature (right, green), and the top 50 genes from human myeloid clusters (center, light pink). (Bottom) Dot plot of the expression of these overlapping genes in CONV-RT and FLASH groups in murine non-resident myeloid cells.

Figure 1

a

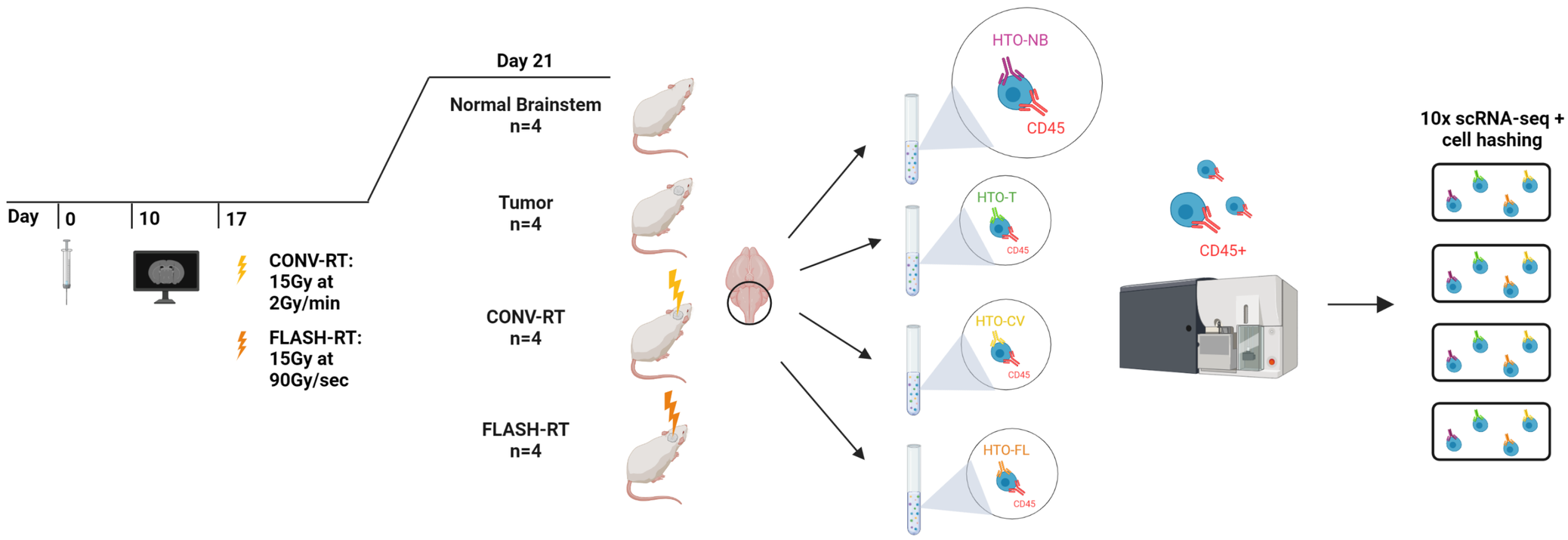

b

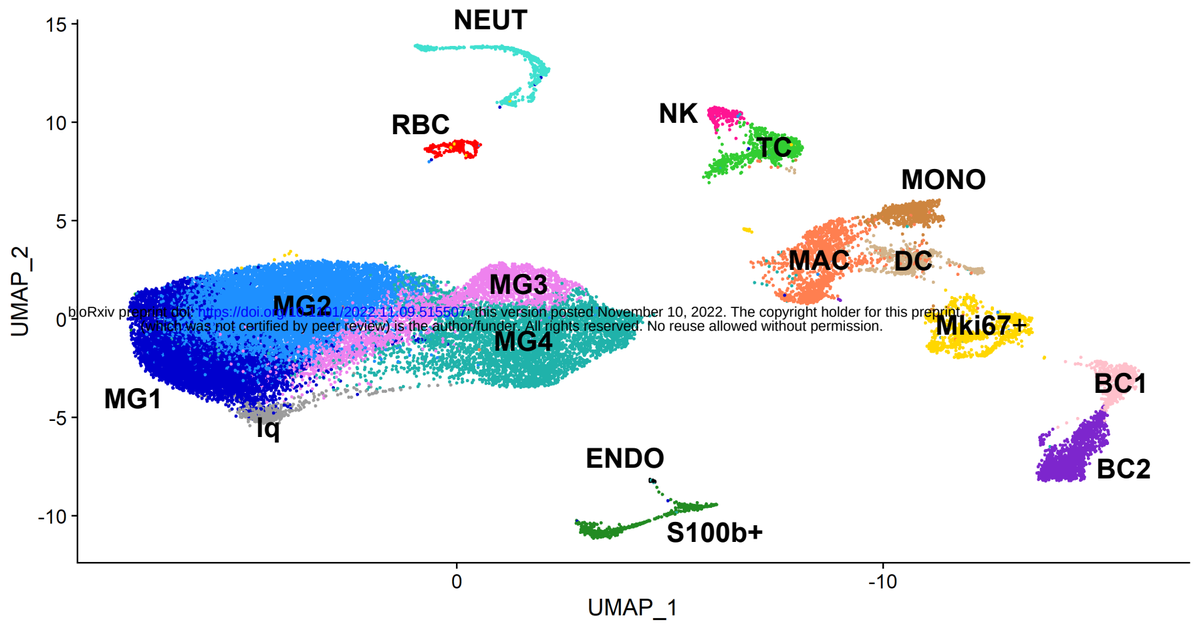

c

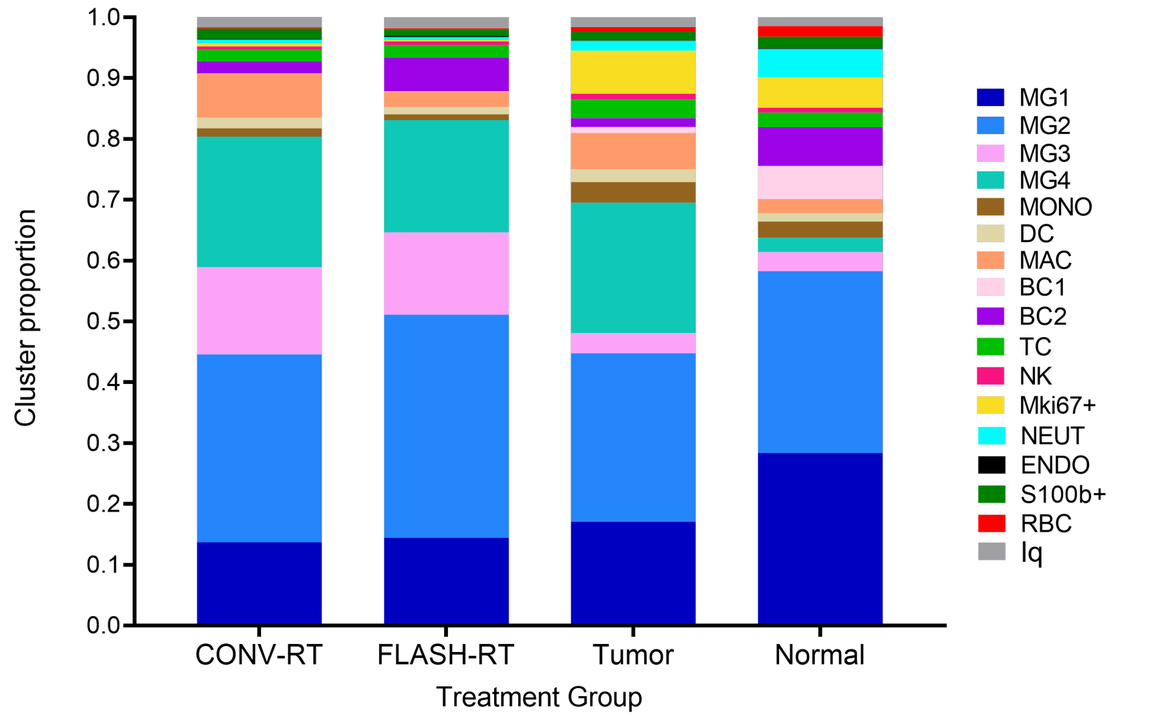

d

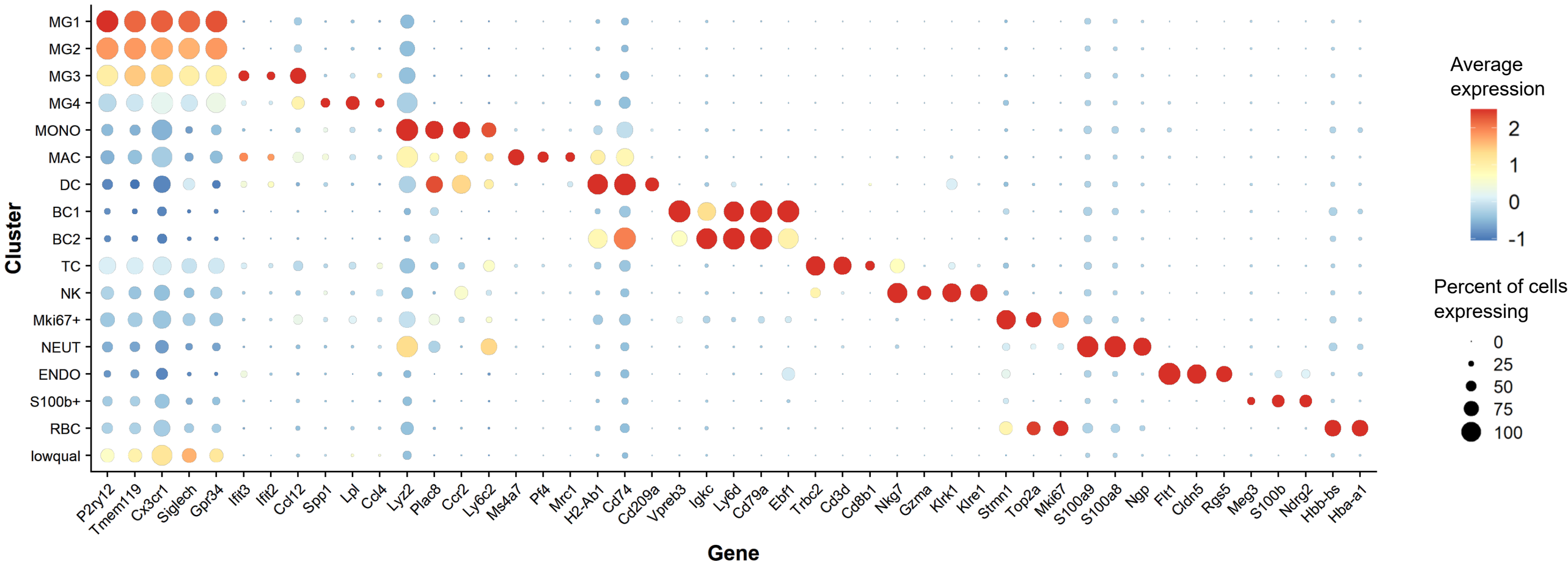

Figure 2

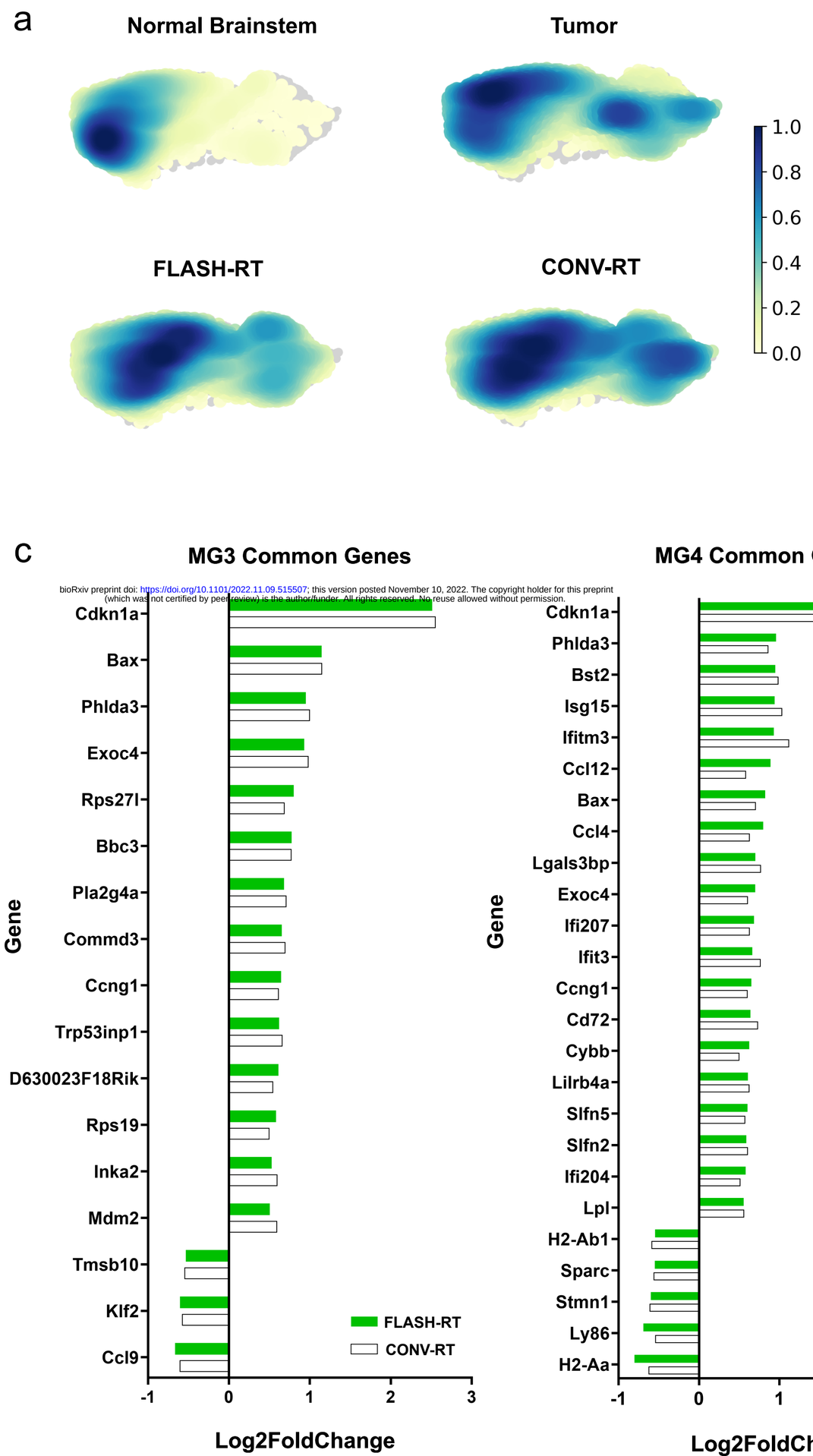

Figure 3

Figure 4

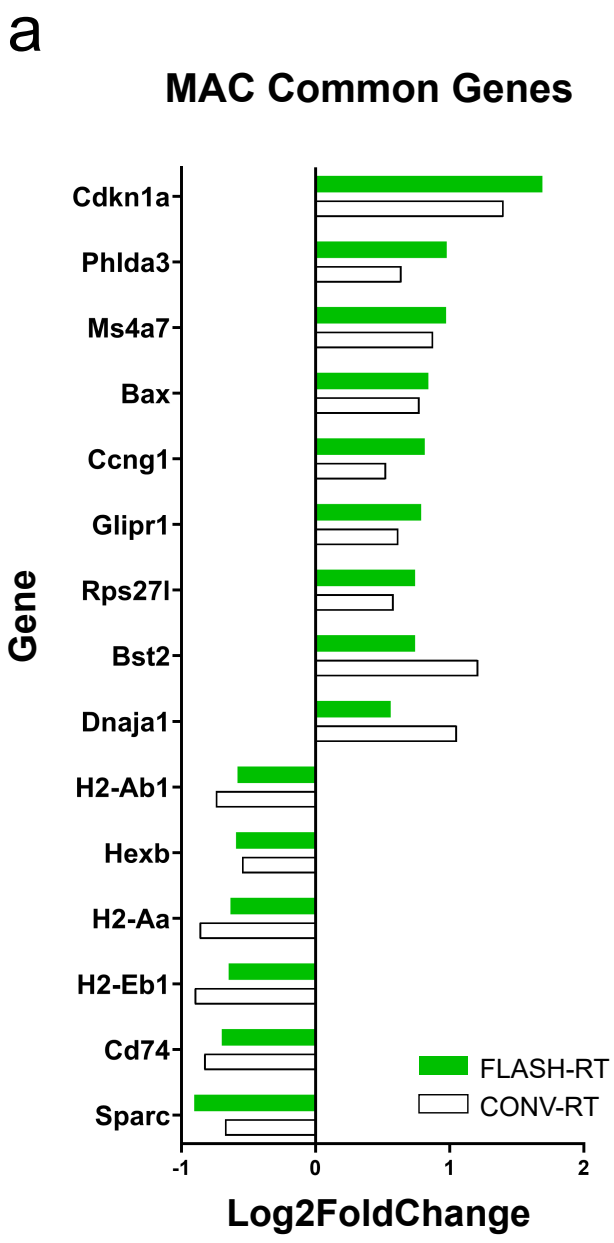

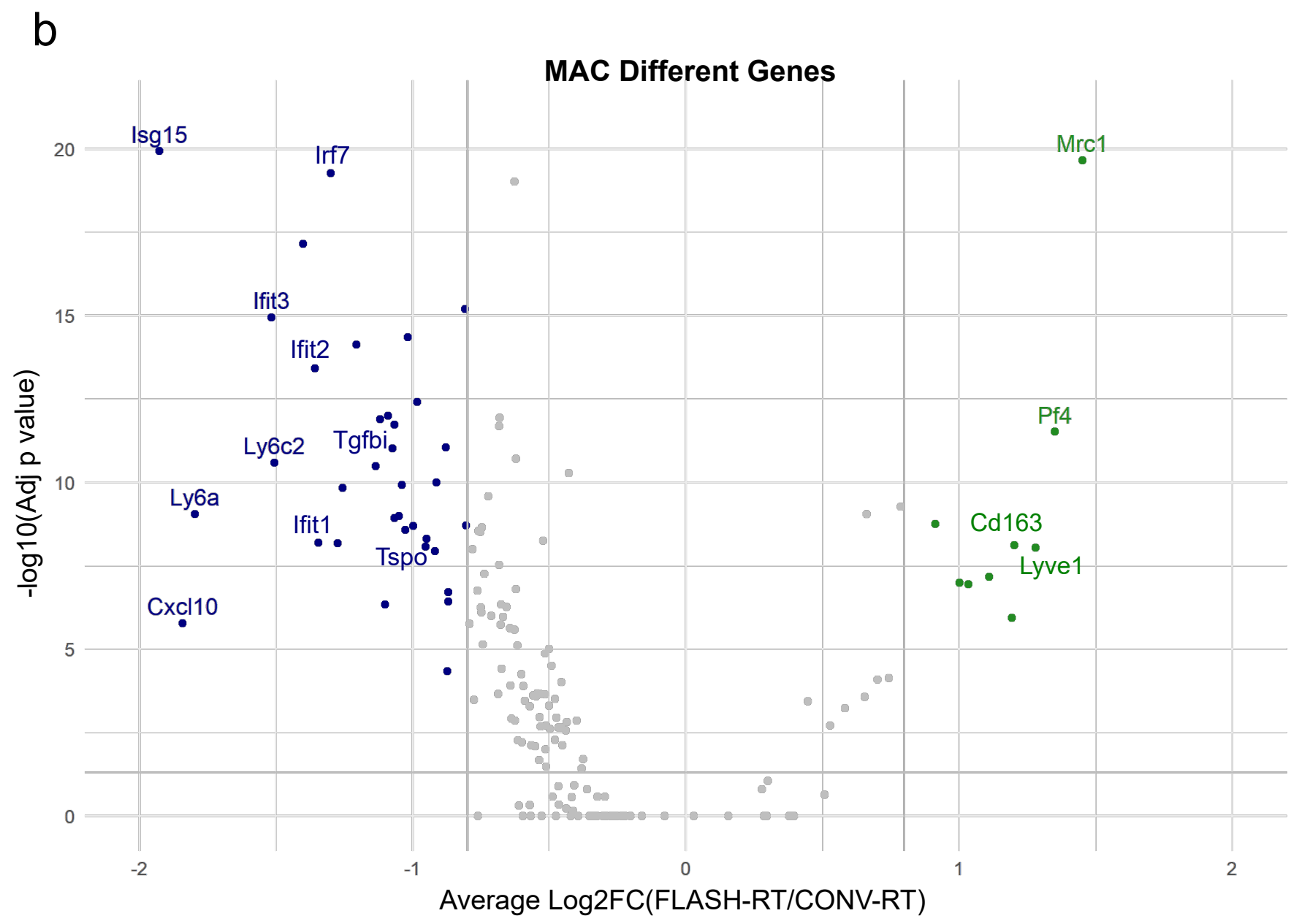

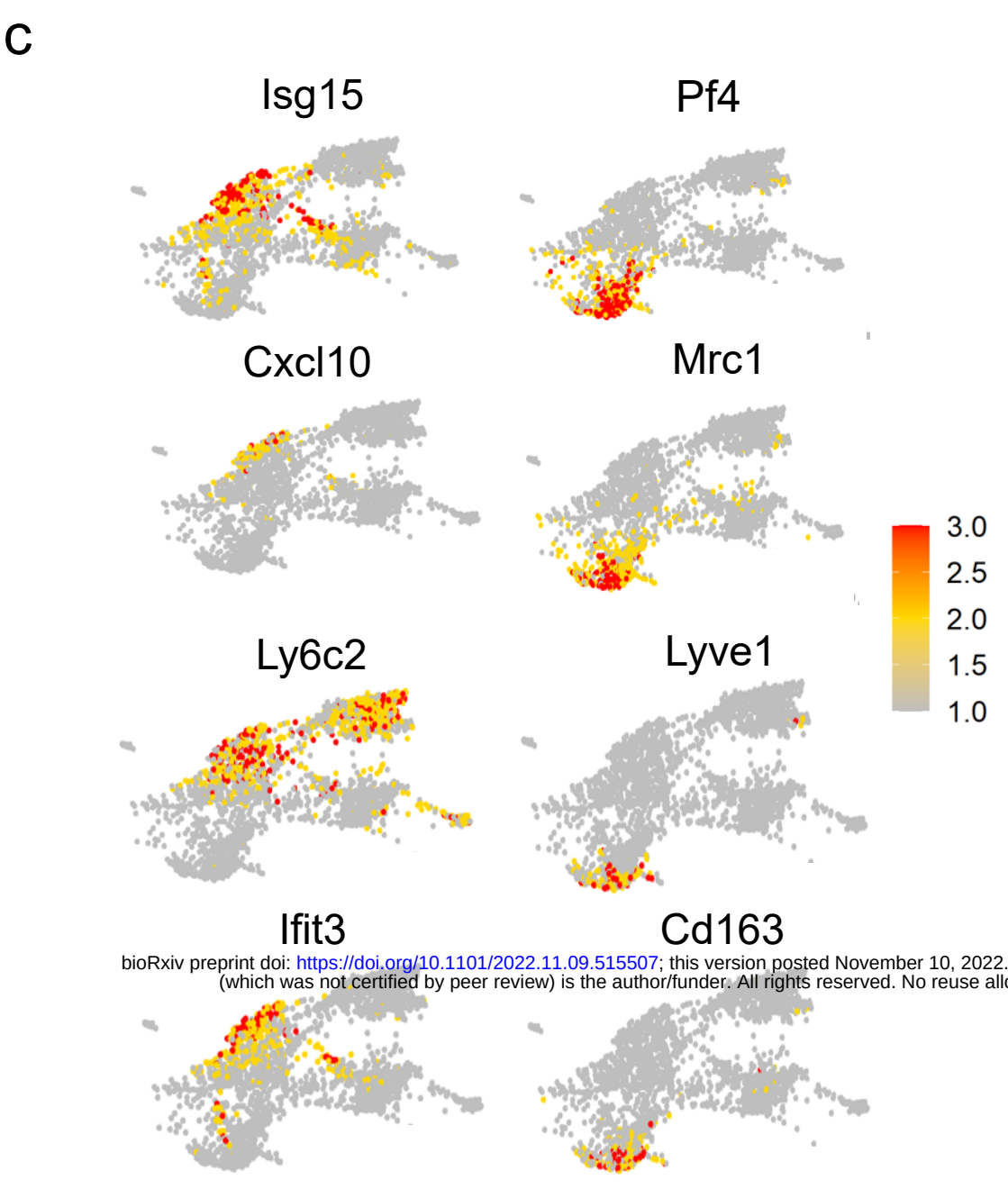

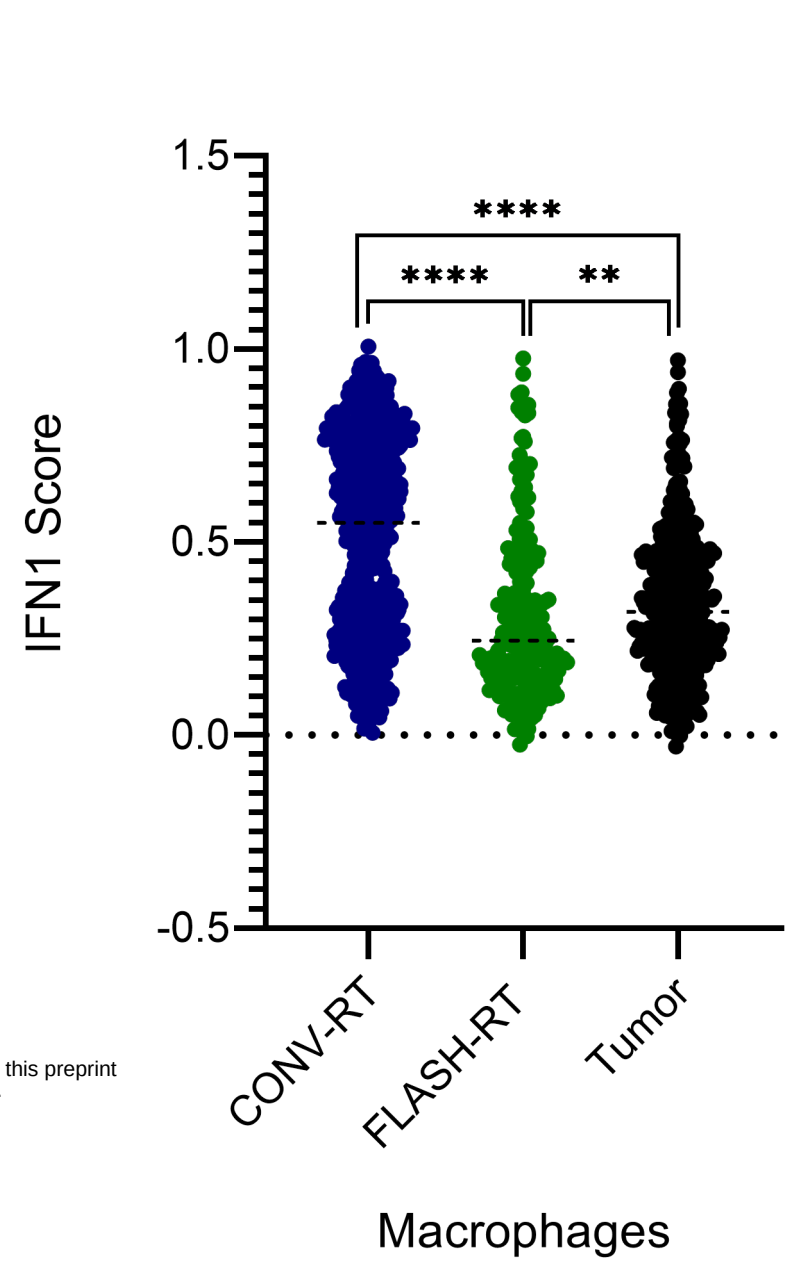

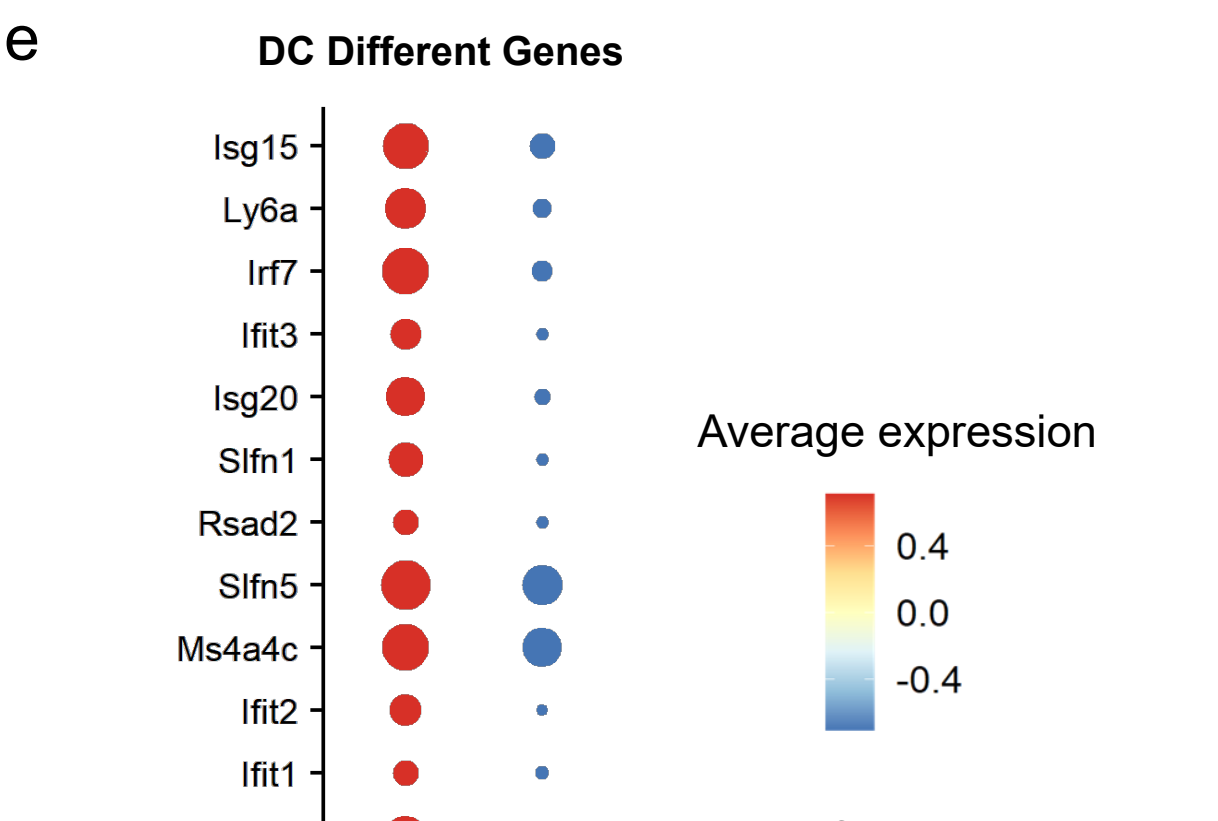

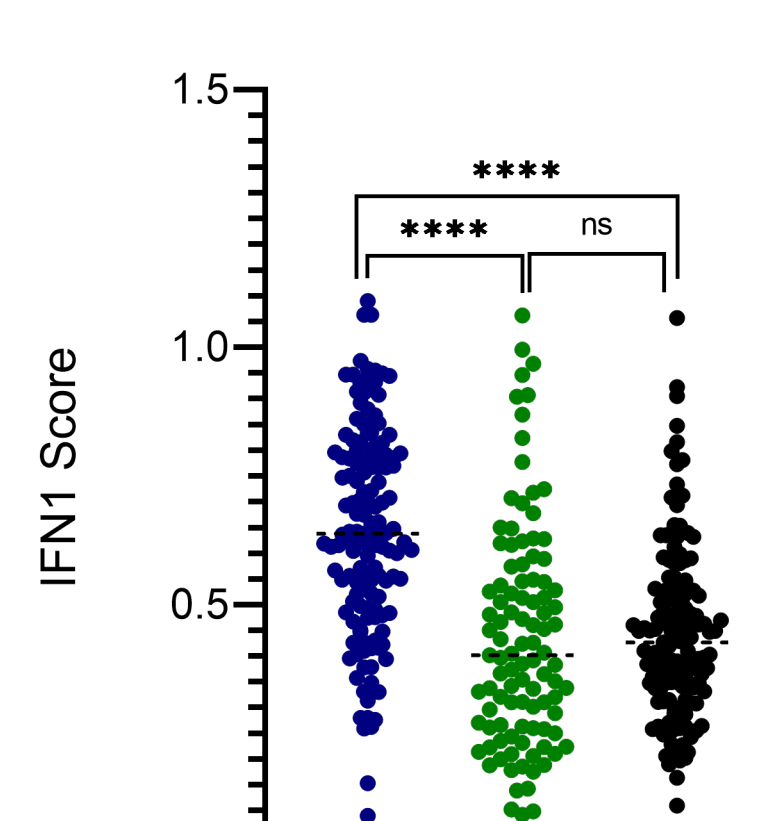

Figure 5

a

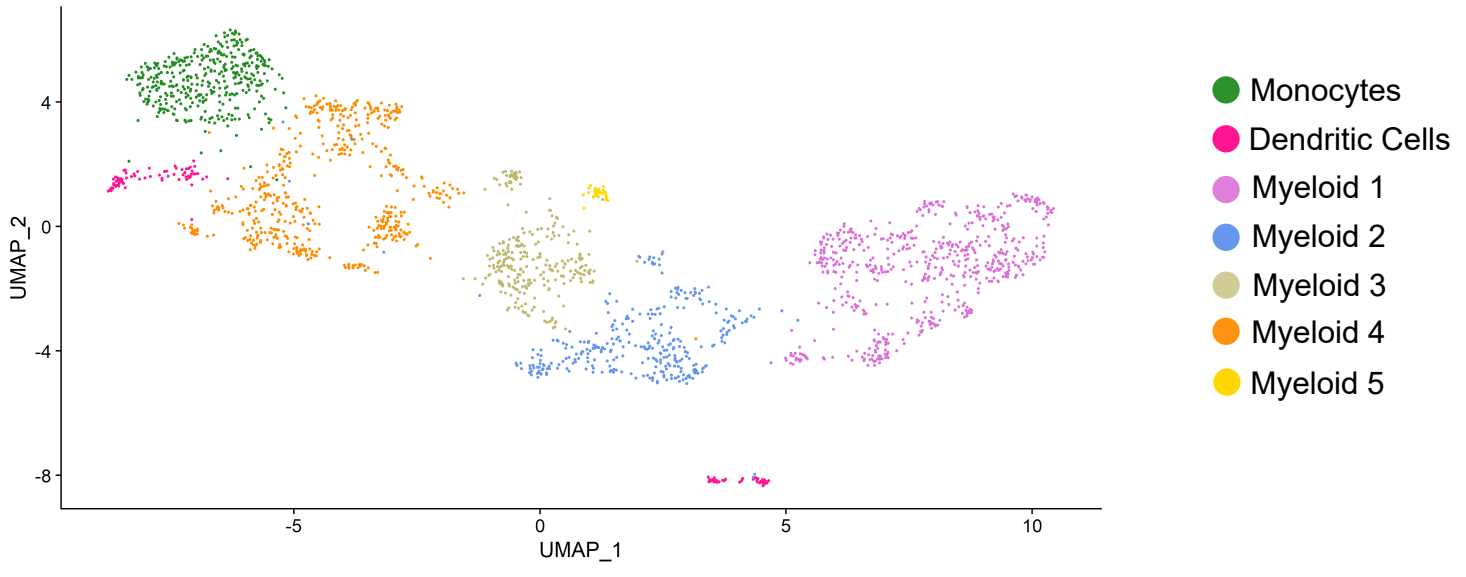

b

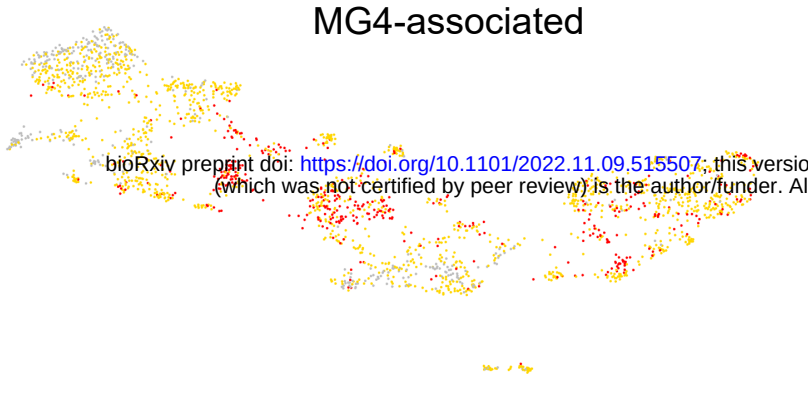

c

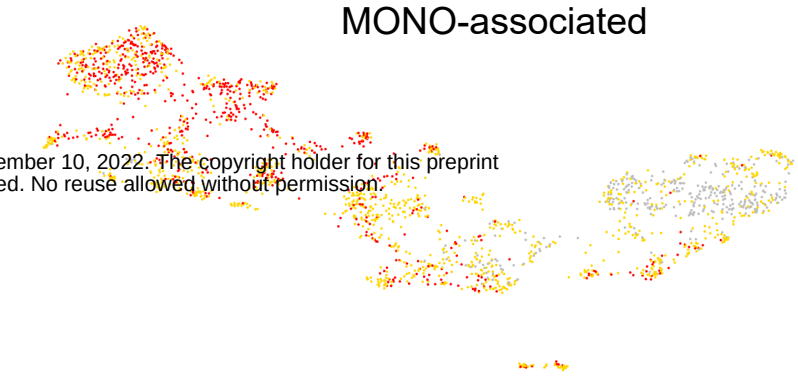

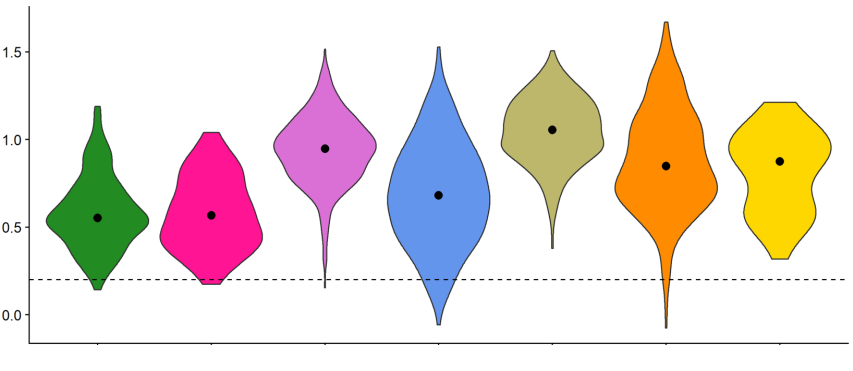

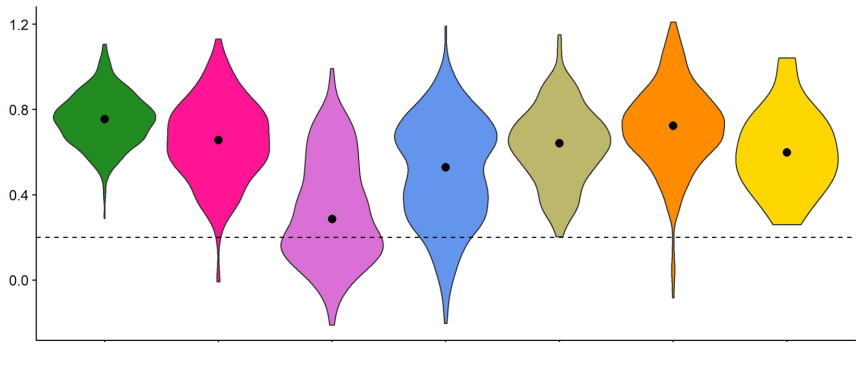

d

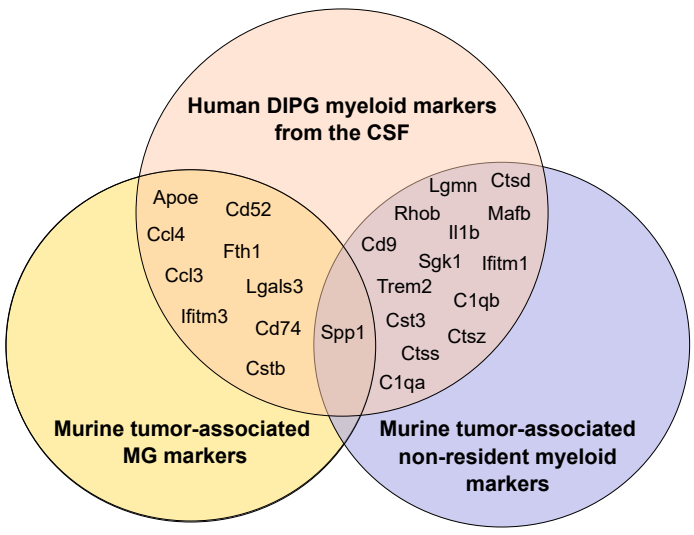

e